Neuron, Vol. 40, 515–525, October 30, 2003, Copyright ©2003 by Cell Press

The Orientation and Molecular Movement of a K^+ Channel Voltage-Sensing Domain

Chris S. Gandhi, Eliana Clark, Eli Loots, Arnd Pralle, and Ehud Y. Isacoff*
Department of Molecular and Cell Biology
271 LSA, MC#3200
University of California, Berkeley
Berkeley, California 94720

Summary

Voltage-gated channels operate through the action of a voltage-sensing domain (membrane segments S1-S4) that controls the conformation of gates located in the pore domain (membrane segments S5-S6). Recent structural studies on the bacterial K_vAP potassium channel have led to a new model of voltage sensing in which S4 lies in the lipid at the channel periphery and moves through the membrane as a unit with a portion of S3. Here we describe accessibility probing and disulfide scanning experiments aimed at determining how well the K_vAP model describes the *Drosophila* Shaker potassium channel. We find that the S1-S3 helices have one end that is externally exposed, S3 does not undergo a transmembrane motion, and S4 lies in close apposition to the pore domain in the resting and activated state.

Introduction

Voltage-gated ion channels conduct ions rapidly and selectively across cell membranes through gated pores. The conformation of these pores is tightly coupled to the membrane potential through a voltage-sensing domain (S1-S4) that regulates the conformation of the pore domain (S5-S6). Several crystal structures of K^+ channels (Doyle et al., 1998; Jiang et al., 2002; Kuo et al., 2003) have confirmed many general features of the pore domain. This domain forms a symmetric tetramer that includes the ion permeation pathway, selectivity filter, and pore gate. S5 and S6 form transmembrane helices arranged so that S5 lies at the periphery of the pore domain while S6 is positioned close to the symmetry axis where it forms a gated constriction near the internal end of the pore. In contrast, relatively little is known about the organization of the voltage-sensing domain or how its movement is functionally coupled to the opening and closing of the pore domain. While there is a consensus that voltage sensing in voltage-gated ion channels is mediated by the movement of positively charged amino acids in the S4 membrane segment, the exact nature of the motion has been the subject of ongoing debate (Bezanilla, 2002; Gandhi and Isacoff, 2002).

The first glimpse of the transmembrane portion of a voltage-gated channel was recently published (Jiang et al., 2003a, 2003b). These studies on the voltage-gated bacterial channel K_vAP led to the proposal of a new model of channel structure and voltage sensing based on a full-length (S1-S6) crystal structure of K_vAP and a structure of the channel's S1-S4 fragment. Although the conformation of S1-S4 differed between these two structures (see Cohen et al., 2003), the structures had in common a close association of S3b with S4, and accessibility analysis indicated that the solution exposure of both S3b and S4 depended on voltage. These observations suggested that S3b and S4 move as a unit in a large transmembrane paddle motion. Since the S1-S4 of the full-length K_vAP structure appeared to be distorted into a nonphysiological conformation, Jiang and colleagues constructed the paddle model by substituting the S1-S4 portion of the full-length structure with the more compact S1-S4 fragment and oriented the fragment by overlapping the S2 helices of the two structures. This placed the charged S4, previously thought to lie partly in a polar protein environment, in the lipid and at the periphery of the channel.

The paddle model is a dramatic departure from voltage-sensing models based on earlier work in eukaryotic K^+ channels. The general principles of the model are depicted in Figures 1A and 1B. In the paddle model, S3b and S4 form a strong association allowing S3b to move transmembrane with S4 as a unit. S2 is buried in the core of the membrane, arranged like a belt around the pore domain. Finally, S4 lies beyond S2 at the periphery of the channel and does not contact the pore domain.

We tested the applicability of the paddle model to the Shaker K^+ channel by asking three questions: (1) does Shaker's S3b move transmembrane with S4?, (2) is Shaker's S2 located in the membrane core?, and (3) is S4 at the channel periphery as proposed in the paddle model or near the pore domain interface as proposed by other models? We addressed the first two questions through an accessibility analysis of S1-S3. The last question was addressed through a disulfide scan between S4 and the pore domain.

Results

Accessibility Analysis on S1, S2, and S3

We tested the membrane disposition of S1-S3 by examining the exposure of single introduced cysteines to externally applied thiol-reactive probes tetramethylrhodamine maleimide (TMRM) and the methanethiosulfonate (MTS) reagents MTSET and MTSES. Each probe is charged and therefore does not readily partition into the hydrophobic membrane.

We first carried out a labeling scan with TMRM and assayed for changes in fluorescence intensity that correlated with changes in membrane voltage. The ability for any particular site to produce a voltage-dependent fluorescence change depends on both the accessibility of that site to TMRM and the chemical environment around that site. We interpreted a change in fluorescence to indicate successful labeling and therefore accessibility. No change in fluorescence intensity was interpreted to indicate either no accessibility *or* labeling at a site that is not in the proper environment for produc-

*Correspondence: eisacoff@socrates.berkeley.edu

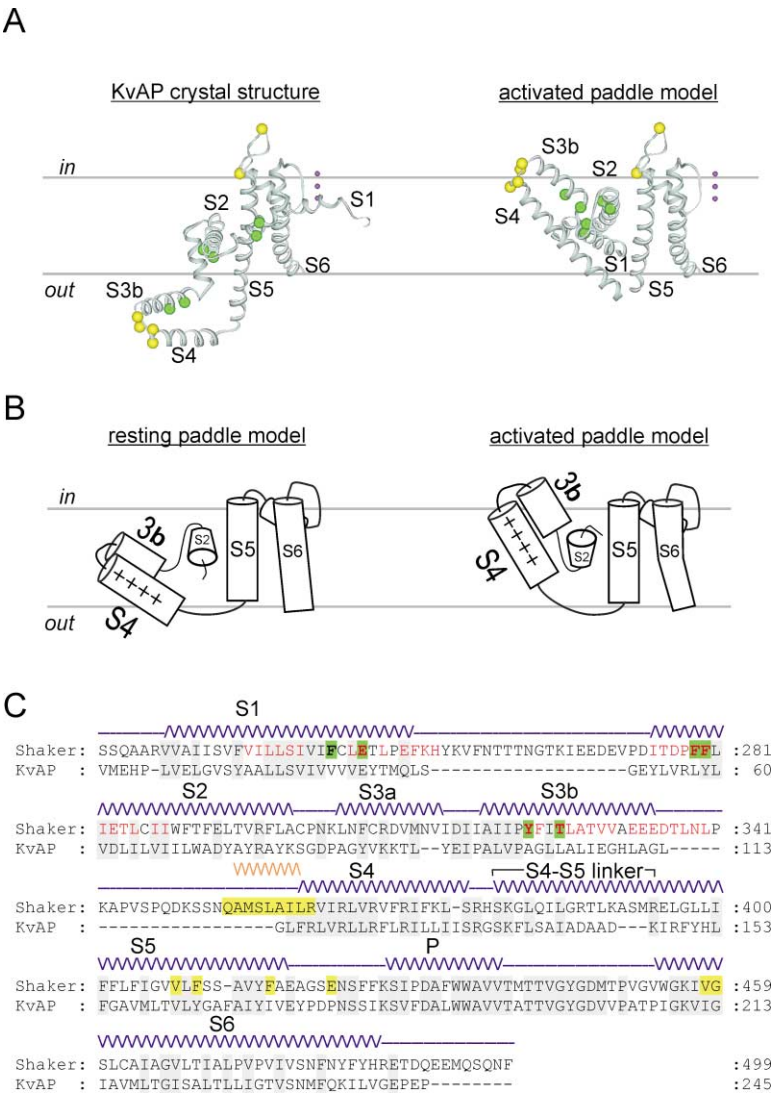

Figure 1. Testing Membrane Topology and Helix Proximity in the Paddle Model

(A) The full-length K_vAP structure and the activated state paddle model are labeled to indicate several sites examined for disulfide bond formation between S4 and the pore domain (yellow) and for state-dependent accessibility to MTS reagents (green). Depiction of the activated state paddle model was adapted from Jiang et al. (2003b). One subunit of the tetrameric channel is shown. Purple spheres indicate K^+ located in the pore. Gray lines indicate the boundaries of the hydrocarbon core of the membrane, which corresponds to a distance of 25 Å (White and Wimley, 1998).

(B) Cartoon representations of the resting and activated state paddle models, based on Figures 5C and 5D of Jiang et al. (2003b).

(C) Sequence alignment of Shaker and K_vAP, indicating sites examined for disulfide bond formation (yellow highlight) and accessibility to external TMRM (red) or MTS reagents (green highlight). Blue zigzag indicates helical segments in the K_vAP structure. Orange zigzag indicates a region in Shaker's S3b-S4 linker deduced to be helical by Gonzalez et al. (2001).

ing a fluorescence change. Therefore, sites that show no fluorescence change cannot categorically indicate inaccessibility. However, a site that does display a voltage-dependent fluorescence change must be accessible to TMRM in some conformation of the channel. Single cysteine mutants were expressed in oocytes and labeled extensively (for 30 min) with a high concentration of TMRM in a depolarizing high K^+ solution. Under these labeling conditions, channels spend time in both resting and activated states. Of 38 single cysteine mutants labeled with external TMRM (Figure 1C), a step of membrane depolarization induced a substantial fluorescence change at 17 sites, indicating access to the charged extracellular probe (Figure 2A). The largest fluorescence changes were observed at the C terminus of S1 and S3b and the N terminus of S2. The results demonstrate that each of these membrane segments has an end that is exposed extracellularly in some conformation of the channel.

To determine the functional state and degree of external exposure, we measured the rate of functional modification of S1-S3 by MTS reagents under voltage clamp. We used voltage protocols with different amounts of time spent at hyperpolarized and depolarized potentials to compare the accessibility of the resting and activated states. Two positions were examined within the boundaries of each helix. These included sites 244 and 247, located between two and three turns from the C-terminal end of the S1 helix; sites 279 and 280, located between two and three turns from the N-terminal end of the S2 helix; and sites 323 and 326, located between three and five turns from the C-terminal end of the S3b helix (Figure 1A).

Two positions in S1 (244 and 247), one position in S2 (280), and two positions in S3b (323 and 326) were all modified at rates similar to previously measured modification of accessible S4 positions (Baker et al., 1998), indicating a high degree of accessibility (Figure 2B). The accessibility of the sites did not differ substantially between the resting and activated states (Figure 2B). An additional site in S2 (279) was modified slowly in both states, as shown previously for a nearby S2 site (283) (Tiwari-Woodruff et al., 2000), indicating that it lies at the limit of accessibility.

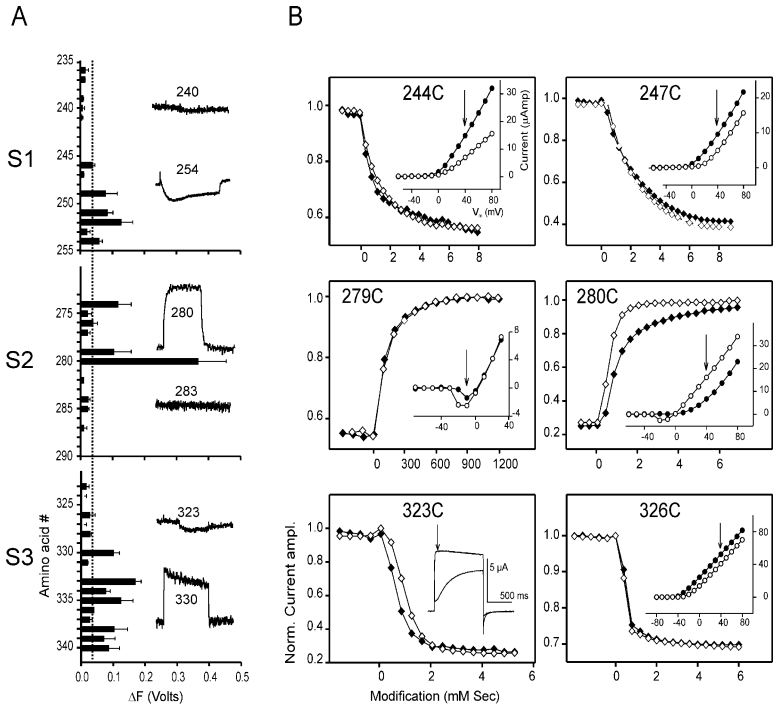

Figure 2. External Accessibility of S1-S3 Cysteines to TMRM and MTS Reagents

(A) Significant ΔFs in response to depolarization from −80 to +40 mV, detected at 17 single cysteine sites in S1, S2, and S3, labeled with external TMRM. Values in the bar graph are mean ± SEM (n = 2–6). Insets show example traces from two sites in each segment. An arbitrary value of $\Delta F \geq 0.035$ V (dashed line) was used as an indication of efficient labeling and, thus, external accessibility.

(B) External accessibility of cysteines to MTSET (244C, 247C, 280C, 326C) and MTSES (279C, 323C) in the resting protocol (closed symbols) and activated protocol (open symbols). Assays were all in the T449V background to prevent slow inactivation. MTS reagents were used at 100 μM for all but 279C, where 5 mM MTSES was used. Insets show current-voltage relation (244C, 247C, 279C, 280C, 326C) or current traces (323C) before (open symbols) and after (closed symbols) MTS exposure. The modification measurement was made at the voltage or time indicated by the arrow. Modification was fast (indicating high accessibility) at all sites except 279C (note differences in x axes). Activated and resting state accessibility was similar at all sites expect 280C, where there was a small reduction in the modification rate at rest.

Rates expressed in $mM^{-1}\ s^{-1}$ as mean ± SEM (n) were (resting protocol/activated protocol) 244C: 1.04 ± 0.08 (3)/0.68 ± 0.04 (4); 247C: 0.64 ± 0.05 (4)/0.73 ± 0.05 (4); 279C: 0.007 ± 0.001 (3)/0.007 ± 0.001 (5); 280C: 1.19 ± 0.11 (3)/1.81 ± 0.12 (3); 323C: 1.48 ± 0.18 (4)/0.93 ± 0.14 (3); 326C: 2.22 ± 0.39 (4)/1.79 ±. 0.20 (4).

Thus, in contrast to the large change in exposure seen previously in S4 (Baker et al., 1998; Larsson et al., 1996; Mannuzzu et al., 1996; Schonherr et al., 2002; Wang et al., 1999; Yang et al., 1996), the C-terminal end of S1, N-terminal end of S2, and much of S3b are exposed externally, and the activation rearrangement does not alter this exposure. The results on Shaker's S3b are in sharp contrast to K_vAP, where S3b becomes inaccessible to the external solution in the resting state (Jiang et al., 2003b).

These results diverge from the paddle model in two significant ways. First, Shaker's S3b does not appear to undergo the transmembrane motion predicted by the paddle model (Figure 1B). Second, Shaker's S2 cannot be embedded within the membrane, since its N terminus is accessible to the external solution in both the resting and activated states.

Disulfide Bond Formation between S4 and the Pore Domain Immobilizes S4

We next employed disulfide scanning to directly determine whether S4 is located at the periphery of the channel as proposed by the paddle model or near the central pore domain as proposed in earlier models. Single cysteines were introduced at positions 354 to 362, which correspond to the N terminus of S4 and the proximal S3-S4 linker. These sites are all externally exposed in the activated state (Baker et al., 1998; Larsson et al., 1996; Mannuzzu et al., 1996; Wang et al., 1999; Yusaf et al., 1996). The S3-S4 linker or S4 cysteine was paired with a second cysteine in S5 (positions 408, 410, or 416), the turret (position 422), or S6 (positions 458 or 459) (Figures 1A and 1C). We then measured the functional effect of oxidizing and reducing agents on channel activity. Each cysteine alone served as a control for the cysteine pair.

In the absence of supplemental oxidizing agents, the double mutation 355C/422C expressed smaller ionic currents than either the 355C or 422C mutation alone, and these currents were increased to the size of single cysteine currents by treatment with the reducing agent DTT (Figure 3A). In addition, both 355C/422C and 359C/416C currents were inhibited by treatment with the oxidizing agent H_20_2 (shown for 359C/416C in Figure 3B). Consistent with a covalent modification, the DTT and H_20_2 effects persisted after washout, and neither DTT nor H_20_2 had a significant effect on the single cysteine mutants, indicating that the cysteine pair was required for the effect (Figures 3A and 3B). These observations are consistent with the spontaneous formation of a disulfide bond between positions 355C and 422C, its reduction by DTT, and the rapid formation of a disulfide bond between positions 355C and 422C and between 359C and 416C in the presence of H_20_2. No inhibition by H_20_2 was detected for double cysteine mutants, which paired position 359 with pore domain sites at the outer end of S6 (458, 459), or deeper in S5 (408, 410) (data not shown), indicating that the interaction is specific. Our results are consistent with the finding that the introduction of a pair of cysteines or histidines in S4 and S5 introduces sensitivity to metals, implying the formation of a metal binding site (Neale et al., 2003; Laine et al., 2003).

The formation of a disulfide bond between S4 and the pore domain is expected to immobilize S4. This should decrease the magnitude of the gating current, as shown

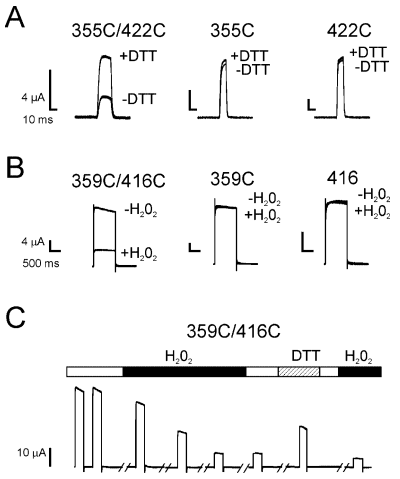

Figure 3. Disulfide Bond Formation between S4 and the Pore Domain

(A) Oocytes incubated in the absence of DTT were voltage clamped. Initial inhibition of 355C/422C current is relieved by DTT (10 mM for 2 min), consistent with the spontaneous formation of a disulfide bond between 355C in the S3-S4 linker and 422C in the turret.

(B) H_2O_2 (0.2% for 2 min) inhibits ionic current of 359C/416C, consistent with formation of a disulfide bond between 359C and 416C, near the outer end of S4 and at the outer end of S5, respectively.

(C) Inhibition of 359C/416C by H_2O_2 persists after washout, is reversed by DTT, and recurs on reapplication of H_2O_2. Responses are to 250 ms depolarizing steps from −110 to +40 mV. Break marks indicate the passage of 1 min. Note that traces for (A) and (B) were obtained in control solution following 1 min washout of the indicated reagent.

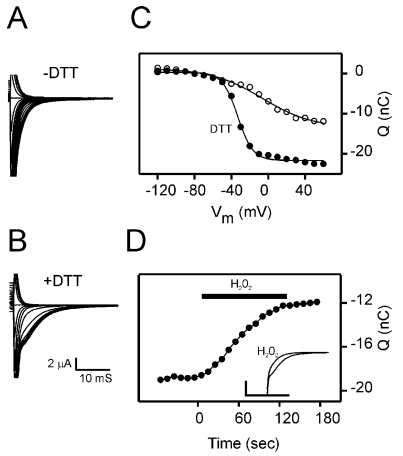

Figure 4. A Disulfide Bond between Positions 355C and 422C Eliminates Gating Current

(A–C) Off-gating current before (A) and after (B) treatment with DTT and voltage dependence of off-gating charge integrated from the gating current (C), before (open symbols) and after (closed symbols) DTT. In the absence of a reducing agent (−DTT) most 355C/422C channels form spontaneous disulfide bonds, and channels have little gating current, indicating an immobilization of S4. Reduction (+DTT) of the disulfide bond (10 mM DTT, 10 min) increases the magnitude of the off-gating current and Charge-Voltage (Q-V) relationship.

(D) Application of H_20_2 (0.2%) reverses the DTT effect and induces cross-linking, which decreases the magnitude of the off-gating charge (Q). Inset shows gating current before and after treatment with H_20_2.

earlier for photoactivated cross-linking of S4 (Horn et al., 2000). We tested this prediction by measuring gating currents in nonconducting (W434F) channels containing the 355C/422C cysteine pair. As expected, DTT *increased* the off-gating current of 355C/422C channels in a manner which persisted after DTT washout (Figures 4A–4C). Subsequent application of H_20_2 *decreased* the off-gating current in a manner that also persisted after washout (Figure 4D). Again, there was no effect on the single mutants 355C or 422C (data not shown). The results indicate that, until at least position 355 (7 residues away from R1 [362]), the Shaker S3-S4 linker is sufficiently structured so that disulfide bond formation to the pore domain prevents the transmembrane movement of S4.

Disulfide Bond Formation on One Face of a Putative α Helix

Next, we carried out a disulfide scan that included positions in the N terminus of S4 and the proximal S3-S4 linker. We confined ourselves to a portion of the S3-S4 linker that is modeled to be helical in Shaker (Gonzalez et al., 2001). Positions 354 through 362 in the S3-S4 linker and S4 were paired with 416C at the external end of S5. H_2O_2 produced a significant inhibition in several but not all of the double mutants (Figure 5). Single cysteine mutants were not sensitive to H_2O_2 (data not shown).

When mapped onto a helical wheel, one face had a slower rate of disulfide bonding (Figure 5A). Site 359—the outermost site known in Shaker to change external exposure with S4 (Baker et al., 1998)—and site 362 (R1) had significant rates of disulfide bond formation to position 416. Very little inhibition was detected at the intervening residue 360, and no inhibition was detected at residue 361. This defines a clear interaction face between this region and the pore domain. Positions 359 and 362 face the pore domain while positions 360 and 361 do not. In the proximal linker, the rates of disulfide bond formation were higher compared to 359 and 362. These high rates were seen on the 359/362 face. However, a significant effect was detected at position 357, which lies on the opposite face. This is consistent with a continuation of the S4 helix into the linker, as proposed earlier (Gonzalez et al., 2001), with perhaps a break in the helix near position 357.

State Dependence of Disulfide Bond Formation

To place constraints on the activation motion of S4, we compared the rates of 359C to 416C disulfide bond formation in the resting and activated states. Current inhibition was rapid when 359C/416C was maintained in the activated state for 50% of the time (Figure 5B). Reducing the activation time to 25% decreased the rate of inhibition to about half. A further reduction to 0.5% activated time decreased the inhibition to a level approaching the background level of the single mutants (Figure 3B). These results indicate that 359C disulfide bonds to 416C only in the activated state. Such behavior could be attributed to either an increase in the resting distance between S4 and S5 or to the lack of external

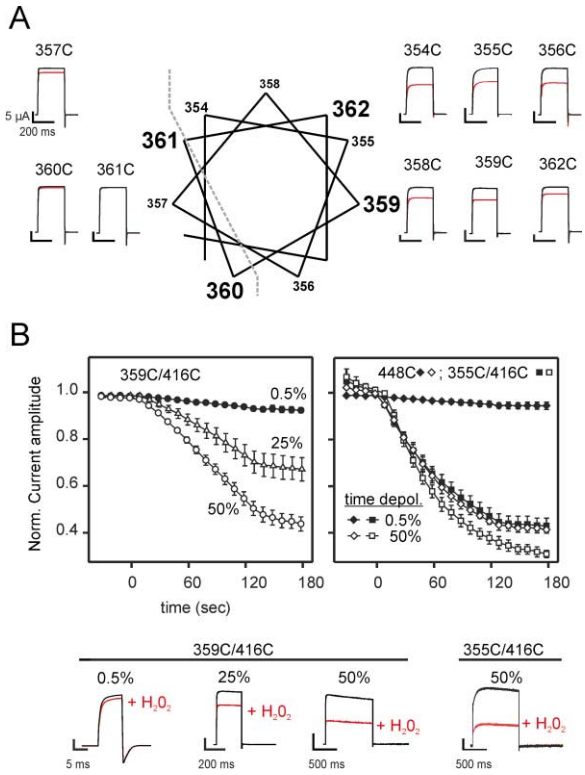

Figure 5. Disulfide Bonding to S5 Depends on the Location of the S3-S4/S4 Cysteine and on the Gating State

(A) The rate of disulfide bond formation was deduced for a series of sites from 354C to 362C paired with 416C in S5 by monitoring the extent of inhibition of the ionic current. Sample traces shown before (black) and after 2 min H_2O_2 (red). When mapped onto a helical wheel, rapid inhibition of current by H_2O_2 is greater for sites on one face of S3b-S4 and S4. The percent of current inhibition after a 2 min exposure to H_20_2 using a 25% duty cycle was 354: 41.0 ± 4.9, n = 11; 355: 40.2 ± 3.4, n = 13; 356: 30.2 ± 2.8, n = 6; 357: 9.1 ± 2.8, n = 14; 358: 10.6 ± 2.8, n = 8; 359: 44.7 ± 3.4, n = 16; 360: 4.4 ± 1.4, n = 9; 361: 0.0 ± 0.0, n = 6; 362: 22.5 ± 6.0, n = 4.

(B) The rate of inhibition of current by H_2O_2 depends strongly on the percentage of time spent depolarized for 359C/416C (top left). The rate was very slow at 0.5% depolarized time and increased when depolarized time was raised to 25% and 50%. For 355C/416C (top right), the rates of inhibition were similar in the resting state (closed squares) and open state (open squares). The rate of inhibition of 355C/416C in both states and of 359C/416C in the activated state were much faster than for intersubunit 448C-448C disulfide bond formation in resting (noninactivated) state (top right, closed diamonds) and comparable for 448C-448C bonding in the C-type inactivated state (top right, open diamonds), suggesting a similar distance between S4 and S5 as the slow inactivated intersubunit distance between 448Cs. Sample traces shown below.

exposure of 359C to oxidizing agent at rest (see Baker et al., 1998).

To distinguish between the above possibilities, we paired the same S5 site, 416C, with 355C, which is externally accessible in both resting and activated states. The rate of H_2O_2 inhibition of 355C/416C in activated channels was faster than that of 359C/416C (Figure 5B). Unlike 359C/416C, the inhibition of 355C/416C in the resting and activated states was similar (Figure 5B, top right panel). Two other pairs, 354C/416C and 356C/416C, also behaved in a similar manner (data not shown).

Because the rate of disulfide bond formation is strongly dependent on the inverse distance between the cysteines (Careaga and Falke, 1992), we could estimate the distance between S4 and S5 by comparing the rates of current inhibition for S4/S5 cysteine pairs to that observed for a cysteine pair of known distance. As a benchmark, we used position 448, which lies at the outer end of the selectivity filter. The distance between 448 β carbons in neighboring subunits is ~13 Å in the structure of the closed KcsA channel (Doyle et al., 1998). In Shaker, intersubunit 448C-448C disulfide bonds have been shown to form slowly in the closed state but form rapidly in the slow inactivated state (Liu et al., 1996), indicating a decrease in the 448 to 448 distance to <13 Å upon inactivation.

H_2O_2 inhibited the 448C currents very slowly in the resting state (Figure 5B, top right panel). In addition, over a 2 min exposure, the amount of inhibition was less than that seen for bond formation between 416 and all of the high-rate sites in S4 and the S3-S4 linker, including Shaker's R1 (362) (Figures 5A and 5B). The rate of inhibition by H_2O_2 was increased considerably in the inactivated state (Figure 5B, top right panel). The 448C-448C inhibition rate for inactivated channels was similar to that seen for 355C-416C in both the resting and activated states, and this rate was approached by 359C-416C in the activated state (Figure 5B). These results suggest that the distances between 448Cs in the inactivated state, 355C-416C in both the resting and activated states, and both 359C-416C and 362C-416C in the activated state are all <13 Å.

Discussion

The membrane topology and organization of voltage-gated channels has long been thought to consist of a tetramer of six membrane-spanning helices. This concept was supported by the findings that the S1-S2 and S3-S4 linkers were accessible to the outside of the cell, the S4-S5 linker was accessible to the inside, and the S1-S2 linker could be glycosylated (Larsson et al., 1996; Mannuzzu et al., 1996; Santacruz-Toloza et al., 1994; Shih and Goldin, 1997). In addition, the charged face of S4 was thought to reside in a partly polar proteinaceous and lipid pocket near the pore domain, and voltage sensing was commonly regarded as primarily a motion of S4 (Durell et al., 1998; Starace and Bezanilla, 2001; Bezanilla, 2002; Gandhi and Isacoff 2002). The crystal structures of K_vAP led to an alternative model of membrane topology and voltage sensing. S2 was placed within the core of the membrane, arranged like a belt around the pore domain, and S4 was proposed to lie at the periphery of the channel and oriented so that its charges faced lipid. In addition, a portion of K_vAP's S3, S3b, was found to move with S4, leading to the general proposal that voltage is sensed via a paddle motion of S3b/S4 moving inward and outward through the membrane. In this work, we attempted to distinguish between these models by measuring the membrane positions and potential transmembrane motion of the S1-S3 helices themselves rather than their linkers. We also asked whether S4 is located within disulfide bonding distance to the pore domain or, as proposed by the paddle model, if S4

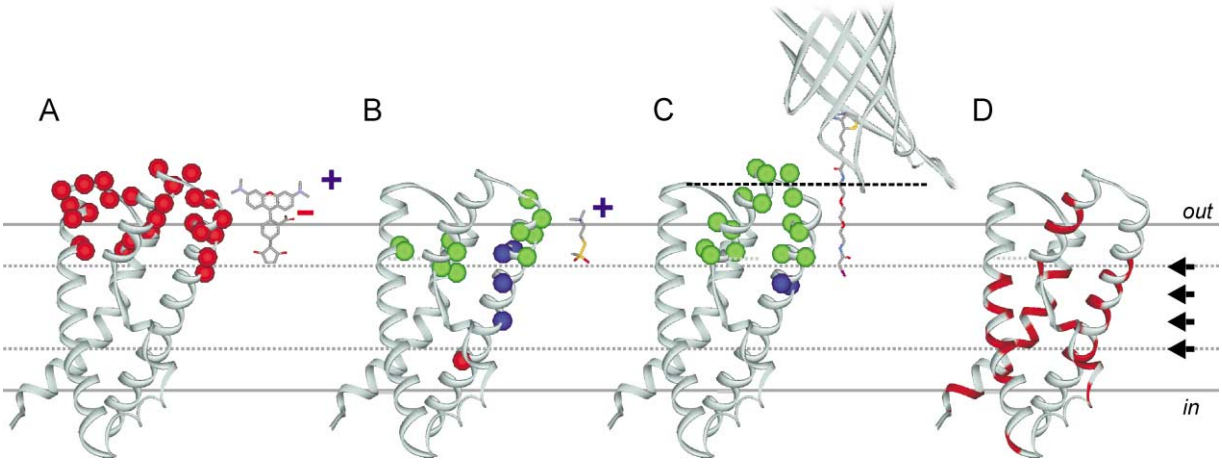

Figure 6. Membrane Topology of the K_vAP S1-S4 Fragment and Possible Interaction Surface with the Pore Domain

(A–C) Activated state accessibility of substituted cysteines to three thiol probes (shown in insets to right of each panel) mapped onto the structure of the K_vAP S1-S4 fragment. Alignment between Shaker and K_vAP is as shown in Figure 1C. Solid gray lines indicate the boundaries of the membrane's hydrocarbon core (White and Wimley, 1998). Dotted gray lines represent the estimated limit of penetration of the maleimide (TMRM) and thiosulfonate (MTSET) reactive groups. (A) Shaker external TMRM accessibility of S1-S3 (from Figure 2A) and S4 (from Gandhi et al., 2000). Red sites are externally accessible, based on the detection of significant voltage-dependent ΔF. (B) Activated state MTS accessibility of Shaker S1-S3 (from Figure 2B) and of Shaker S4 to MTSET or pCMBS (from Larsson et al., 1996; Baker et al., 1998; Wang et al., 1999; green is externally accessible, blue is externally inaccessible, magenta is internally accessible). (C) Activated-state accessibility of external Avidin (top ribbon, truncated) to biotin-thiol linker conjugated to a K_vAP cysteine (from Jiang et al., 2003b). Note, Avidin is shown to approach only as far as the channel surface (dotted black line).

(D) Sites where mutation perturbs gating (red backbone) in Shaker and $K_v2.1$ (Monks et al., 1999; Hong and Miller, 2000; Li-Smerin et al., 2000; Li-Smerin and Swartz, 2001) map to the packed core of the K_vAP S1-S4 fragment and to the surface of S4 (arrows), consistent with the outer face of S4 interacting with the pore domain. The high perturbation outer face of S4 is continuous with the face of S4 that disulfide bonds to the pore domain.

might be in the channel periphery and thus too distant to disulfide bond to the pore domain. Finally, our results place distance and topology constraints on the structure and activation mechanism of the Shaker channel, which we reconcile with the crystal structures of K_vAP.

Membrane Topology of S1-S3

We found that multiple residues at the C-terminal ends of S1 and S3b and the N-terminal of S2 were accessible to external TMRM under conditions where channels populated a mixture of functional states. In addition, when we examined voltage-clamped channels in either the resting or activated state, residues located well within each of these helices were exposed to external MTS reagents. This exposure was similar in the resting and activated states; therefore, the C terminus of S1, the N terminus of S2, and much of S3b are always exposed to the external solution, regardless of the conformational state of the channel. While the accessibility results clearly define a membrane topology for S1-S3 in the resting and activated states, they do not preclude a movement of these segments. It is important to consider that any movement of S1-S3 that does not alter the exposure of those segments will not be detected by an accessibility analysis. Even with this caveat, it is clear that neither S1, S2, and in particular S3b move in a transmembrane motion.

The accessibility results were mapped onto the structure of the K_vAP S1-S4 fragment. TMRM exposure in S1-S3 determined here was combined with earlier observations on S4 fluorescence (Figure 6A), and MTS exposure of S1-S3 was combined with earlier observations on S4 accessibility in the activated state (Figure 6B). The Shaker TMRM and MTS accessibility maps define a zone of overlapping positions that include the C termini of S1 and S3 and the N termini of S2 and S4. These results indicate a membrane orientation quite different from the paddle model. Interestingly, our Shaker orientation is compatible with the activated state accessibility measurements on K_vAP when one takes into account that the target (in this case a biotinylated cysteine) can only be accessed by the probe (Avidin) if the target is less than 10 Å from the membrane *and* the neighboring protein surface (Figure 6C).

We also superimposed our Shaker accessibility results onto the resting and activated state conformations predicted by the paddle model (Figure 7A). Shaker MTS accessibility was reasonably compatible with the activated state paddle model. The major exception was S1, which is not explicitly located in the paddle model but whose location can be inferred from the predicted position of S2 (Jiang et al., 2003b). However, our Shaker accessibility results are clearly not compatible with the resting state paddle model. Positions in Shaker's S1-S3 which we find to be externally accessible are predicted to lie at a similar membrane location as inaccessible positions in K_vAP's S3b and S4 (Jiang et al., 2003b) and Shaker's S4 (Baker et al., 1998).

Thus, our analysis identifies an important divergence in behavior between Shaker and the predicted behavior of the paddle model. The paddle model predicts that S3b and S4 undergo a joint transmembrane motion; however, in Shaker only S4 undergoes a transmembrane motion. Moreover, our accessibility analysis demonstrates

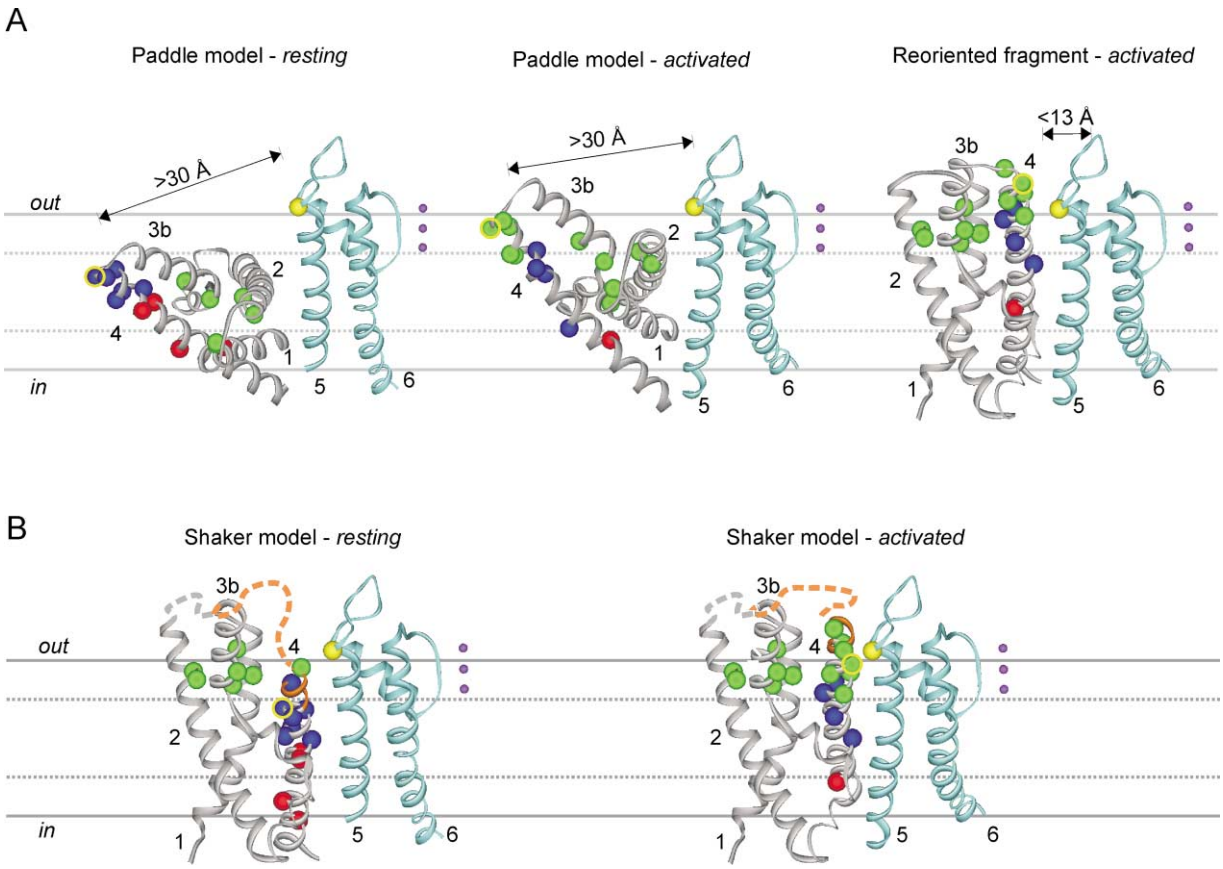

Figure 7. Accessibility and Disulfide Bonding Results Mapped Suggest an Alternative to the Paddle Model

(A) Shaker accessibility and disulfide bonding sites mapped onto the resting (left) and activated state (middle) conformations of the paddle model (see Experimental Procedures) and onto an alternative model in which the structure of the K_vAP S1-S4 fragment is reoriented. One subunit of the tetrameric channel is shown. Purple spheres indicate K^+ ions in the pore of the channel. Accessibility sites and membrane boundaries are depicted as in Figure 6. Sites which are externally accessible in S1, S2, and S3 (green) are located in the resting paddle model at the same membrane depth as S4 sites that are inaccessible (blue) or accessible to the inside (red), indicating that the paddle model does not account for the resting state membrane topology of Shaker. There is a better agreement between Shaker accessibility and the activated paddle model (middle). The distance between R1 (S4) and 416 (S5) is >30 Å in both the resting and activated conformations of the paddle model (right, center), not consistent with the observation of rapid disulfide bonding. Reorientation of the K_vAP S1-S4 fragment in the membrane and with respect to the pore domain agrees with both the accessibility and disulfide analyses on Shaker (right). The accessibility of S4 in the K_vAP S1-S4 fragment and the interaction between positive charges in S4 and negative charges in S2 and S3 (Tiwari-Woodruff et al., 2000) are both consistent with the activated state.

(B) The voltage-sensing motion of Shaker's S4 is depicted for the reoriented fragment (A, right), with S4 moving alone at the interface with S5. S4 moves without a transmembrane motion in S1, S2, or S3b. Activation displaces S4 sites that are inaccessible (blue) to the outside (green) and sites that are accessible internally (red) into an inaccessible location (blue). S4 here includes a helical extension of 6 residues at the outer end of S4, up to residue 355.

that the paddle model cannot adequately describe the membrane topology of the Shaker channel, and we suggest an alternative membrane orientation of Shaker's S1-S4 based on the structure of K_vAP's S1-S4 fragment.

Location of S4 at the Interface between the Voltage-Sensing and Pore Domains

Our disulfide scanning showed a high rate of disulfide bonding between positions in the proximal S3-S4 linker or S4 and one position at the outer end of S5. The alignment of the R1 of Shaker (362) with the R1 of K_vAP (117) (Figure 1C) places Shaker position 362 within K_vAP's S4 helix. Shaker position 359 is only 2 residues from the end of the K_vAP helix and, thus, close to the position of S4. Both positions are only accessibly to external oxidizing agents in the activated state; therefore, disulfide binding between these positions and S5 provides a good indication of the activated state location of S4.

The interpretation of the results for the resting state depends on the structure of the proximal S3-S4 linker in Shaker. This will determine how well position 355 represents the location of S4. The crystal structure of K_vAP cannot inform us as to the secondary structure of Shaker's S3-S4 linker, since K_vAP only contains a 4 residue linker that forms a tight hairpin turn, while Shaker has a linker of 26 residues (Figure 1). In Shaker, the linker has been modeled to extend as a helix from S4 to at least position 355 (Gonzalez et al., 2001). This model is consistent with our finding that sites with a higher rate of disulfide bond formation to S5 map onto one face of a continuous helix extending from S4 to

the proximal S3-S4 linker (Figure 5A). Two additional observations indicate that the proximal S3-S4 has an ordered structure that is rigidly associated with S4. First, fluorophores conjugated to positions in S4 and the proximal S3/S4 linker manifest similar changes in fluorescence that correlate to channel activation, implying that the linker and S4 undergo a similar activation motion (Gandhi et al., 2000). Second, disulfide bonding of position 355 to a position in the pore domain immobilizes the gating charge carried by S4 (Figure 4). Together these observations suggest that the proximal S3-S4 linker moves with S4 and is likely in a compact secondary structure that places position 355 close to the end of S4.

The distance between S4 and the pore domain was estimated through a rate comparison of bond formation between a pair of cysteines of known distance and our S3/S4 and S5 cysteines. We estimate the distance between the proximal S3-S4 linker and S5 to be $<$13 Å in the activated state. This analysis also indicates that in the resting state, when the outer end of S4 moves inward away from the external surface, position 355 in the proximal S3-S4 remains $<$13 Å from the outer end of S5. Thus, it appears that the activation rearrangement does not move the S3-S4 linker far from S5.

Due to differences between the conformation of S1-S4 in the two crystal structures of K_vAP, it has been suggested that the S1-S4 domain is inherently flexible and can adopt many conformations (Jiang et al., 2003a), at least in detergent. Such flexibility could mean that S4 might be able to reach many locations scattered far and wide over the channel. While it is conceivable that S4 may visit many conformations, occupancy of any conformation that deviates considerably from the average native position will be brief and rare and would result in slow disulfide bonding rates. The rapid disulfide bond formation that we observe between S3-S4/S4 and S5 (Figures 3–5) indicates a considerable fraction of time spent at close range, consistent with a high proximity average position. Indeed, the range appears to be similar to or closer than that known to exist for the intersubunit bond between nearby positions in the selectivity filter, a structure that does not appear to be particularly flexible, given the similarity in selectivity filter structure between the apparently closed KcsA (Doyle et al., 1998) and the apparently open K_vAP (Jiang et al., 2003a). In keeping with this interpretation, we found that position 359 showed specificity in disulfide bonding with the pore domain, since it could not disulfide bond to positions in S6 or deeper in S5.

The high rates of disulfide bonding between the proximal S3-S4 linker and S5 and between S4 and S5 appear to reflect the specific spatial proximity of S4 to S5 in both the resting and activated states. This suggests that the transmembrane motion of S4 takes place at the interface between the voltage-sensing and pore domains. The short distances between S4 and S5 are not compatible with either the resting or the activated conformations of the paddle model. Due to the placement of S2 between S4 and the pore domain, the S4-S5 distance is always greater than 30 Å in both paddle model conformations (Figure 7A), well beyond the distances over which rapid disulfide bond formation has been observed (Careaga and Falke, 1992).

Model of Voltage-Sensing Domain Structure and Motion in the Shaker Channel

Our findings indicate that the K_vAP paddle model cannot account for the structure or activation motion of the Shaker channel for the following reasons: (1) S3b and S4 do not move transmembrane as a unit, (2) S2 is not located in the core of the membrane, and (3) S4 is located close to S5 and not at the channel periphery. In Shaker, the transmembrane motion of S4 takes place with little apparent change in the distance between its proximal linker and S5 and with little to no change in the external accessibility of S1, S2, and S3b. These results are more compatible with a transmembrane voltage-sensing motion of S4 alone.

By reorienting the structure of the K_vAP S1-S4 fragment in the membrane, we already showed that we could account for both the Shaker and K_vAP accessibility measurements (Figures 6A–6C). To arrive at a structural model of Shaker voltage sensing, we took this membrane orientation of the S1-S4 fragment and docked it onto the pore domain of K_vAP using the proximity constraints from our disulfide bond measurements (Figure 7A). In this configuration, S1-S4 traverses the entire depth of the membrane and the positively charged portion of S4 that is buried in the span of the membrane faces counter-charges in S2 and S3a. A transmembrane motion of S4 alone in the z axis of the membrane can account for Shaker's voltage-dependent accessibility change, our disulfide bonding results, and the lack of transmembrane motion of S1-S3 (Figure 7B). It is interesting to note that a similar motion involving the translation of a helix in the z direction of the membrane has been inferred from crystal structures of the Ca^{2+} pump in two different conformations (Toyoshima and Nomura, 2002).

Our docking model is compatible with several observations on eukaryotic K_v channels. First, in many K^+ channels, including Shaker, the C-terminal end of S3b bears as many as four negative charges, and their deletion in Shaker does not prevent gating (Gonzalez et al., 2001). Several groups report that each Shaker subunit moves the equivalent of three to four positive S4 gating charges completely through the membrane during activation (Aggarwal and MacKinnon, 1996; Schoppa et al., 1992; Seoh et al., 1996). However, the paddle model predicts that four negative charges on S3b would move transmembrane as a unit with S4, neutralizing much of the gating charge. Permanent external exposure of a negatively charged S3b would prevent neutralization of the gating charge. Second, in Shaker and $K_v2.1$, most mutations that strongly perturb channel opening and therefore were predicted to lie at protein-protein interfaces (Hong and Miller, 2000; Li-Smerin et al., 2000; Li-Smerin and Swartz, 2001; Monks et al., 1999) map to protein contacts within the K_vAP S1-S4 fragment structure. High perturbation sites in general do not map to the surface of the fragment, with the exception of one face of S4 (Figure 6D). This suggests that this surface of S4 forms a protein-protein contact with another part of the channel and is not exposed primarily to lipid. Third, electrostatic interaction between Shaker S4's R362 and E418 near the end of S5 has been calculated to occur over a distance of $\sim$8 Å (Elinder et al., 2001), and introduction of cysteine or histidine pairs into S4

and S5 introduces sensitivity to metal ions, implying sufficient proximity to form bivalent coordination sites (Neale et al., 2003). Finally, the external location of S2's N-terminal end is consistent with tolerance of the insertion of a highly charged epitope tag at the N-terminal end of S2 (Shih and Goldin, 1997).

The recently proposed paddle model makes specific predictions regarding the membrane placement of S2, the transmembrane motion of S3b, and the location of S4 at the periphery of the channel. Using accessibility analysis, we have shown that the α-helical portions of S1-S3 have one end that is exposed to the external solution and that exposure does not depend on the conformational state of the channel. Therefore, S2 cannot be located in the core of the membrane as proposed by the paddle model, where it would be inaccessible to both externally applied MTS and TMRM. In addition, S3b cannot undergo a transmembrane motion, since its accessibility to external MTS is not state dependent. The absence of a unified S3b/S4 transmembrane motion in Shaker indicates that a strong association between S3b and S4 is not universal among K^+ channels, a finding consistent with the lack of sequence conservation in S3b or of S3b-S4 linker length (Cohen et al., 2003). Finally, using disulfide scanning, we find that S4 is located near S5 in both the resting and activated state of the channel and not at the periphery of the channel as proposed by the paddle model.

Taking into account the crystal structures of KvAP and the above results, we propose an alternative model of voltage sensing and channel structure (Figure 7B). We predict that S2 spans the entire length of the membrane, demonstrate that S3b does not undergo a transmembrane motion, and show that S4 lies at the interface between the voltage-sensing and pore domains. Our model arranges S1-S6 as membrane-spanning helices organized with S1 and S2 located near the periphery of the channel and S4 adjacent to S5. Activation displaces S4 through the membrane and does not alter the external exposure of positions within the S1-S3 helices. Therefore, we propose that the essential motion of voltage sensing is a transmembrane motion of S4 alone.

Experimental Procedures

Molecular Biology

Experiments were performed on ball-deleted ShH4 (Δ6-46) T449V (to block N-type and C-type inactivation; Hoshi et al., 1990; Lopez-Barneo et al., 1993) Shaker channels after substitution of two native cysteines (C245V and C462A). Additional mutations for accessibility and cross-linking measurements were built onto this "wild-type" background. Gating current measurements were conducted in the "wild-type" plus W434F (to block ionic conduction; Perozo et al., 1993) plus 449T background. Site-directed mutagenesis, complementary RNA synthesis, and cRNA injection into *Xenopus* oocytes were performed as described (Gandhi et al., 2000).

Electrophysiology

Oocyte recordings were performed as described (Gandhi et al., 2000). Recording solutions consisted of 110 mM NaMes, 11 mM KMes, 2 mM $CaMes_2$, 10 mM HEPES (pH 7.4). For experiments that required measurement of inward current, 60 or 110 KMes was used and the NaMes concentration was reduced to maintain osmolarity. Preparation of MTS stock and accessibility measurements were performed as described (Larsson et al., 1996). For disulfide bond experiments, oocytes were incubated overnight in 100 μM DTT, washed in control solution, and recorded in recording solution supplemented with either 0.2% H_20_2 (oxidizing conditions) or 10 mM DTT (reducing conditions). Traces shown are always after a 1 min washout in control solution.

Voltage-Clamp Fluorometry

Voltage-clamp fluorometry and oocyte preparation and incubation were performed as described (Gandhi et al., 2000). Oocytes were labeled by incubation with either 5 μM or 50 μM 6′-TMRM for 30 min on ice then stored at 18°C in the dark until measured.

Accessibility Protocols

Oocytes expressing S1, S2, or S3 cysteine mutants were assayed for a change in the gating property specified (Figure 2B) upon application of MTS. The protocols used are (V_{test} ms/V_h ms) (% time depolarized): (10 ms/2000 ms) (0.5%); (1000 ms/2000 ms) (50%). $V_{hold} = -110$ mV, $V_{test} = +40$ or -10 mV. MTS was used at a concentration of 100 μM for all positions with the exception of 5 mM for 279C.

Disulfide Scanning Protocols

Oocytes expressing double cysteine mutants were pretreated with DTT to reduce disulfide bonds that formed spontaneously, extensively washed, and then assayed for a decrease in ionic current upon application of H_2O_2. A 250 ms test pulse was applied once every second, thus allowing the channels to spend 25% time at the activated voltage (+40 mV) and 75% time at the resting voltage (-110 mV). Slow inactivation was inhibited by the T449V mutation. The protocols used are (V_{test} ms/V_h ms) (% time depolarized): (10 ms/2000 ms) (0.5%); (250 ms/1000 ms) (25%); (1000 ms/2000 ms) (50%). $V_{hold} = -110$ mV, $V_{test} = +40$ mV. 448C channels were tested using a 50% depolarized protocol in the 449T background to place channels in the slow inactivated state (inactivation τ 60 ms) or the 0.5% protocol to minimize inactivation and keep channels largely in the resting (closed) state. All S3-S4 positions tested, with the exception of 361C, result in complete current inhibition under oxidizing conditions when paired against 416C; therefore, the rates of disulfide bonding were compared by measuring the extent of current inhibition after a 2 min exposure to 0.2% H_20_2 using the 0.5%, 25%, or 50% protocols. Oxidizing conditions did not inhibit the current of 359C paired against 458C, 459C, 408C, or 410C, indicating that inhibition is specific.

Construction of Structural Models

To reconstruct the paddle model, we began by performing a structural alignment of S2 from K_vAP's S1-S4 fragment against S2 from the full-length K_vAP structure. S1-S4 from the full-length structure was then removed, and the fragment was rotated about the center of S2 in order to approximate Figures 5C and 5D in Jiang et al. (2003b). The resting state conformation of the pore domain was modeled by aligning the K_vAP S5 and S6 to the conformations of the TM1 and TM2 of KcsA (Doyle et al., 1998). While we were able to reproduce the activated state depicted in Jiang et al. (2003b) through a simple rigid body transformation of the K_vAP S1-S4 fragment structure (Figure 7A, middle panel), we could not exactly reproduce their depiction of the resting state without making internal rearrangements within the fragment. We approximated the resting paddle orientation as best as possible without performing internal rearrangements through a second rigid body transformation (Figure 7B, left panel). For simplicity, we show our models complete with S1 helices, even though these have steric clashes with the pore domain. Portions of S1 that clash with the pore domain are not rendered in our depiction of the paddle model. In the original model, Jiang et al. (2003b) note that S1's position is indeterminate. However, the membrane disposition of S1 can be inferred from the position of S2. Although our depictions of the paddle model differ from the original depiction by Jiang et al. (2003b), the essential elements of the model including the placement of S2, the location of S4 at the channel periphery, the transmembrane motion of S3b together with S4, and the relative depth in the membrane of S2, S3b, and S4 provide a close approximation.

The resting and activated state of our final model was created by orienting the structure of K_vAP's S1-S4 fragment to account for

Shaker and K_vAP accessibility measurements on S1-S4. To account for our disulfide bond results, the reoriented fragment was then docked against the pore domain of K_vAP so that the N terminus of S4 was within 6–8 Å of the external end of S5 (Figure 7A, right panel). It should be noted that a small rotation of the S1-S4 fragment can enable the S4-S5 linker to bridge S4 either to the S5 within the same subunit or a neighboring subunit (as suggested recently by Laine et al., 2003). The final resting and activated conformation of S4 was created by taking our reoriented model and translating S4 in the z direction of the membrane (Figure 7B) while simultaneously rotating S4 about its helical axis to produce a helical screw motion. The mean position of S4 moves ~14 Å in the z direction of the membrane to account for the large state-dependent changes in S4 accessibility measured previously (Baker et al., 1998; Larsson et al., 1996; Mannuzzu et al., 1996; Wang et al., 1999; Yang et al., 1996; Yusaf et al., 1996). In the resting state, 359 (same face as 362, see Figure 7B) is positioned below and pointing away from 416. Activation rotates S4 so that 359 and 362 now face 416. Position 355, which is one turn and 40 degrees away from 359, moves from a resting position that is slightly below 416 to an activated position that is slightly above it. In effect, we have chosen our rearrangement so that 355 is equidistant from 416 in both states and so 359 approaches 416 only in the activated state. We have rendered the backbone from position 355 to the end of S3b as a dashed line to indicate ambiguous secondary structure. The state independence of 355 to 416 disulfide bonding could also be due to a state-dependent flexibility in the end of the S3/S4 helix predicted by Gonzalez et al. (2001); however, we do not think the segment becomes unstructured. If this were the case, disulfide bond formation would not completely abolish the ionic and gating current. It should also be noted that a movement only in the z direction (i.e., no helical twist) could also account for our disulfide bonding results. In this model, the 359/362 face of S4 would always points toward S5.

Acknowledgments

We thank Medha Pathak for initiating the MTS experiments; Dan McGee, Sandra Wiese, and Lisa Kurtz for valuable technical assistance; Medha Pathak, Francesco Tombola, James Berger, Kathleen Collins, Richard Kramer, John Ngai, Diane Papazian, and members of her lab for helpful discussion; and T.R. Ogdor for manuscript preparation. The work was supported by NIH R01NS35549, Packard Foundation 99-8325, and a postdoctoral fellowship from HFSP to A.P.

Received: August 14, 2003
Revised: September 9, 2003
Accepted: September 22, 2003
Published: October 29, 2003

References

Aggarwal, S.K., and MacKinnon, R. (1996). Contribution of the S4 segment to gating charge in the Shaker K+ channel. Neuron *16*, 1169–1177.

Baker, O.S., Larsson, H.P., Mannuzzu, L.M., and Isacoff, E.Y. (1998). Three transmembrane conformations and sequence-dependent displacement of the S4 domain in shaker K+ channel gating. Neuron *20*, 1283–1294.

Bezanilla, F. (2002). Voltage sensor movements. J. Gen. Physiol. *120*, 465–473.

Careaga, C.L., and Falke, J.J. (1992). Structure and dynamics of Escherichia coli chemosensory receptors. Engineered sulfhydryl studies. Biophys. J. *62*, 209–216.

Cohen, B.E., Grabe, M., and Jan, L.Y. (2003). Answers and questions from the KvAP structures. Neuron *39*, 395–400.

Doyle, D.A., Morais Cabral, J., Pfuetzner, R.A., Kuo, A., Gulbis, J.M., Cohen, S.L., Chait, B.T., and MacKinnon, R. (1998). The structure of the potassium channel: molecular basis of K+ conduction and selectivity. Science *280*, 69–77.

Durell, S.R., Hao, Y., and Guy, H.R. (1998). Structural models of the transmembrance region of voltage-gated and other K+ channels in open, closed, and inactivated confromations. J. Struct. Biol. *121*, 263–284.

Elinder, F., Mannikko, R., and Larsson, H.P. (2001). S4 charges move close to residues in the pore domain during activation in a K channel. J. Gen. Physiol. *118*, 1–10.

Gandhi, C.S., and Isacoff, E.Y. (2002). Molecular models of voltage sensing. J. Gen. Physiol. *120*, 455–463.

Gandhi, C.S., Loots, E., and Isacoff, E.Y. (2000). Reconstructing voltage sensor-pore interaction from a fluorescence scan of a voltage-gated K+ channel. Neuron *27*, 585–595.

Gonzalez, C., Rosenman, E., Bezanilla, F., Alvarez, O., and Latorre, R. (2001). Periodic perturbations in Shaker K+ channel gating kinetics by deletions in the S3–S4 linker. Proc. Natl. Acad. Sci. USA *98*, 9617–9623.

Hong, K.H., and Miller, C. (2000). The lipid-protein interface of a Shaker K(+) channel. J. Gen. Physiol. *115*, 51–58.

Horn, R., Ding, S., and Gruber, H.J. (2000). Immobilizing the moving parts of voltage-gated ion channels. J. Gen. Physiol. *116*, 461–476.

Hoshi, T., Zagotta, W.N., and Aldrich, R.W. (1990). Biophysical and molecular mechanisms of Shaker potassium channel inactivation. Science *250*, 533–538.

Jiang, Y., Lee, A., Chen, J., Cadene, M., Chait, B.T., and MacKinnon, R. (2002). Crystal structure and mechanism of a calcium-gated potassium channel. Nature *417*, 515–522.

Jiang, Y., Lee, A., Chen, J., Ruta, V., Cadene, M., Chait, B.T., and MacKinnon, R. (2003a). X-ray structure of a voltage-dependent K+ channel. Nature *423*, 33–41.

Jiang, Y., Ruta, V., Chen, J., Lee, A., and MacKinnon, R. (2003b). The principle of gating charge movement in a voltage-dependent K+ channel. Nature *423*, 42–48.

Kuo, A., Gulbis, J.M., Antcliff, J.F., Rahman, T., Lowe, E.D., Zimmer, J., Cuthbertson, J., Ashcroft, F.M., Ezaki, T., and Doyle, D.A. (2003). Crystal structure of the potassium channel KirBac1.1 in the closed state. Science *300*, 1922–1926.

Laine, M., Lin, M.C., Bannister, J.P., Silverman, W.R., Mock, A.F., Roux, B., and Papazian, D.M. (2003). Atomic proximity between S4 segment and pore domain in Shaker potassium channels. Neuron *39*, 467–481.

Larsson, H.P., Baker, O.S., Dhillon, D.S., and Isacoff, E.Y. (1996). Transmembrane movement of the shaker K+ channel S4. Neuron *16*, 387–397.

Li-Smerin, Y., and Swartz, K.J. (2001). Helical structure of the COOH terminus of S3 and its contribution to the gating modifier toxin receptor in voltage-gated ion channels. J. Gen. Physiol. *117*, 205–218.

Li-Smerin, Y., Hackos, D.H., and Swartz, K.J. (2000). alpha-helical structural elements within the voltage-sensing domains of a K(+) channel. J. Gen. Physiol. *115*, 33–50.

Liu, Y., Jurman, M.E., and Yellen, G. (1996). Dynamic rearrangement of the outer mouth of a K+ channel during gating. Neuron *16*, 859–867.

Lopez-Barneo, J., Hoshi, T., Heinemann, S.H., and Aldrich, R.W. (1993). Effects of external cations and mutations in the pore region on C-type inactivation of Shaker potassium channels. Receptors Channels *1*, 61–71.

Mannuzzu, L.M., Moronne, M.M., and Isacoff, E.Y. (1996). Direct physical measure of conformational rearrangement underlying potassium channel gating. Science *271*, 213–216.

Monks, S.A., Needleman, D.J., and Miller, C. (1999). Helical structure and packing orientation of the S2 segment in the Shaker K+ channel. J. Gen. Physiol. *113*, 415–423.

Neale, E.J., Elliott, D.J., Hunter, M., and Sivaprasadarao, A. (2003). Evidence for inter-subunit interactions between S4 and S5 transmembrane segments of the shaker potassium channel. J. Biol. Chem. *278*, 29079–29085.

Perozo, E., MacKinnon, R., Bezanilla, F., and Stefani, E. (1993). Gating currents from a nonconducting mutant reveal open-closed conformations in Shaker K+ channels. Neuron *11*, 353–358.

Santacruz-Toloza, L., Huang, Y., John, S.A., and Papazian, D.M. (1994). Glycosylation of shaker potassium channel protein in insect cell culture and in Xenopus oocytes. Biochemistry *33*, 5607–5613.

Schonherr, R., Mannuzzu, L.M., Isacoff, E.Y., and Heinemann, S.H. (2002). Conformational switch between slow and fast gating modes: allosteric regulation of voltage sensor mobility in the EAG K+ channel. Neuron *35*, 935–949.

Schoppa, N.E., McCormack, K., Tanouye, M.A., and Sigworth, F.J. (1992). The size of gating charge in wild-type and mutant Shaker potassium channels. Science *255*, 1712–1715.

Seoh, S.A., Sigg, D., Papazian, D.M., and Bezanilla, F. (1996). Voltage-sensing residues in the S2 and S4 segments of the Shaker K+ channel. Neuron *16*, 1159–1167.

Shih, T.M., and Goldin, A.L. (1997). Topology of the Shaker potassium channel probed with hydrophilic epitope insertions. J. Cell Biol. *136*, 1037–1045.

Starace, D.M., and Bezanilla, F. (2001). Histidine scanning mutagenesis of basic residues of the S4 segment of the shaker K+ channel. J. Gen. Physiol. *117*, 469–490.

Tiwari-Woodruff, S.K., Lin, M.A., Schulteis, C.T., and Papazian, D.M. (2000). Voltage-dependent structural interactions in the Shaker K(+) channel. J. Gen. Physiol. *115*, 123–138.

Toyoshima, C., and Nomura, H. (2002). Structural changes in the calcium pump accompanying the dissociation of calcium. Nature *418*, 605–611.

Wang, M.H., Yusaf, S.P., Elliott, D.J., Wray, D., and Sivaprasadarao, A. (1999). Effect of cysteine substitutions on the topology of the S4 segment of the Shaker potassium channel: implications for molecular models of gating. J. Physiol. *521*, 315–326.

White, S.H., and Wimley, W.C. (1998). Hydrophobic interactions of peptides with membrane interfaces. Biochim. Biophys. Acta *1376*, 339–352.

Yang, N., George, A.L., Jr., and Horn, R. (1996). Molecular basis of charge movement in voltage-gated sodium channels. Neuron *16*, 113–122.

Yusaf, S.P., Wray, D., and Sivaprasadarao, A. (1996). Measurement of the movement of the S4 segment during the activation of a voltage-gated potassium channel. Pflugers Arch. *433*, 91–97.